Rios, S., Cristelo, C., Viana da Fonseca, A., Ferreira, C. (2016). Stiffness behavior of a soil stabilized with alkali activated fly ash from small to large strains. International Journal of Geomechanics, DOI: 10.1061/(ASCE)GM.1943-5622.0000783. (http://ascelibrary.org/doi/abs/10.1061/(ASCE)GM.1943-5622.0000783)

Stiffness behavior of a soil stabilized with alkali activated fly ash from small to large strains

Sara Rios [a]; Nuno Cristelo [b]; António Viana da Fonseca [c]; Cristiana Ferreira [d]

[a] Post-Doc Research Fellow (corresponding author), CONSTRUCT-GEO, Faculty of Engineering of the University of Porto
E-mail: sara.rios@fe.up.pt

[b] Assistant Professor, CQVR, School of Science and Technology, University of Trás-os-Montes e Alto Douro

[c] Associate Professor, CONSTRUCT-GEO, Faculty of Engineering of the University of Porto,

[d] Assistant Professor, CONSTRUCT-GEO, Faculty of Engineering of the University of Porto

Abstract

Alkaline activation of fly ash creates a geopolymeric cement that can replace the ordinary Portland cement in several applications such as soil improvement, with the advantage of much lower CO_2 emissions and reusing an industrial by-product otherwise landfilled, thus averting several environmental problems. In this paper, the behavior of a silty sand improved by the alkaline activation of fly ash is analyzed from small to large strains by presenting uniaxial and drained triaxial compression tests' results, as well as seismic wave velocities measured throughout the curing period. The dynamic, cyclic and static tests show a significant increase in stiffness with curing time, even beyond the 28 days of curing period. Based on the non-destructive wave propagation technique, the increase of the shear and compression wave velocities with time were drawn giving the evolution of the elastic shear modulus as well as the Poisson ratio values. The dynamic Young modulus was compared to the correspondent secant Young modulus obtained from the mechanical tests. Additionally, the evolution of the properties of this stabilized soil with curing time was compared and confronted to that of soil-cement, based on the elastic stiffness of both materials, showing that the most significant difference lies on the curing rate.

Keywords: Fly-ash, Alkaline activation, Soil improvement, Triaxial tests, Seismic Wave Measurements

Introduction

Soil stabilization with cement and/or lime-based binders has been the subject of many research programs over the last few decades (e.g., Dupas and Pecker, 1979; Little, 1995; Camusso and Barla, 2009; Consoli et al., 2011; Rios et al., 2012; Houssain and Yin, 2014; Rahimi et al., 2016). Recently, other materials have been tested successfully for artificially cementation of soils, like biopolymers (Chen et al., 2014; Khatami and O'Kelly, 2013), polymer-infused roots (Sauceda et al., 2014), carbonating reactive magnesia (Yi et al., 2013) or microbial-induced calcite precipitation (e.g., Cheng et al., 2013). The interest in soil improvement is based on the environmental, economic, social and technical advantages of improving the geotechnical properties of the original soil, instead of, for instance, replacing it by a soil with better mechanical properties. However, environmental issues related to cement production and durability concerns regarding its application to a soil layers constitute a significant motivation to develop new binders. In particular, the amount of carbon dioxide released to the atmosphere by the cement industry is estimated to represent 5% to 8% of the global carbon dioxide emissions (Scrivener and Kirkpatrick, 2008). In that sense, the use of increasing volumes of waste materials, such as fly ash (Kang et al., 2016) in the construction industry is becoming a more and more significant contribution for the reduction in cement consumption.

Several studies have recently been made aiming the characterization of alkali activated fly ash as a possible substitute for traditional Portland cement from the mechanical and environmental point of view (e.g., Palomo et al., 1999; Turner and Collins, 2013). However, most of them are focused on structural applications, as a substitute for concrete (e.g., Bernal et al., 2011). The few studies for soil improvement applications were only based on a high consumption of alkaline activator (Cristelo et al., 2011, 2013, Sukmak et al., 2013), and the final product was a viscous grout, with an almost liquid consistency, very different from that of a typical soil-

cement mixture. The mechanical behavior of these mixtures is therefore far from that of a lightly cemented soil. The high levels of activator have also a significant impact on the cost of the technique, producing strength levels which can be much higher than needed.

Therefore, this research project intended to characterize the geotechnical behavior of a well graded silty-sand resulted from remolded residual soil from granite masses, abundant in Porto region, stabilized with fly ash (FA) activated with low rates of a sodium-based grout. The low rates of activator are expected to have three major consequences:

- The generation of lower strength levels than those reported in the scarce available literature regarding soil stabilization with alkali activated fly ash, but still high enough for most geotechnical applications.
- The lower percentages of activator will reduce the total cost of the technique, to a level for what it becomes competitive with cement from a financial point of view.
- It will also produce a final mixture with a soil-like structure, which will enable the use of common geotechnical laboratory tests and procedures, namely in the triaxial apparatus.

In the present paper, the deformation behavior of this stabilized soil is assessed based on uniaxial and triaxial tests – using local strain instrumentation; and seismic wave analysis - using ultrasonic transducers, throughout the loading process, from very small to very large shear strains. This large range characterization is essential to accurately predict the stress-strain behavior, enabling the design of geotechnical structures with this material. Considering the extensive worldwide experience of soil-cement behavior (Rios et al., 2014), a comparison between both materials is presented.

Materials and Methods

This study presents the characterization of mixtures composed by silty sand (characterized in Viana da Fonseca et al., 2013), fly ash and an alkaline activator. Low calcium content fly ash (Class F according to ASTM C618, 2003), produced by a Portuguese coal-fired thermo-electric power plant, was used. The activator was prepared using a sodium silicate (SS) to sodium hydroxide (SH) ratio of 1:2. The SS was originally in solution form, with a bulk density of 1.464 g/cm^3 at 20ºC, a SiO_2/Na_2O weight ratio of 2.0 (molar oxide ratio of 2.063) and a Na_2O concentration in the solution of 13.0%. The SH was originally supplied in pellets with a specific gravity of 2.13 at 20ºC (99 wt%), and was dissolved in water to form a 7.5 molal solution.

Three types of mixtures were studied, with different FA percentages (relatively to the total solids weight), activator contents (liquid to solids ratio) and dry unit weights. Furthermore, specimens with the same ash contents and a liquid phase constituted solely by water, that is, without activator, were molded and tested for comparison purposes. Characterization of all the fabricated mixtures is shown in Table 1. More details may be found in Rios et al. (2016).

To fabricate the specimens, the dry soil was first mixed with fly ash until a homogeneous mixture was obtained. Then, the activator solution (produced 6 h before use to allow temperature stabilization) was added, followed by further mixing. The resulting paste was compacted in three layers inside a cylindrical stainless steel mold with 70 mm of diameter and 140 mm height in order to obtain the desired unit weight. After 48 h the specimen was removed from the mold and wrapped in cling film, to avoid moisture loss, before being stored again in a controlled temperature room (20ºC). Curing periods of 28 and 90 days were considered.

Uniaxial compression strength (UCS) and drained triaxial compression (CD) tests were performed according to ASTM 1633 (1996) and ASTM D7181 (2011), respectively, on specimens cured for 28 (UCS and CD) and 90 days (UCS). A 100-kN automatic hydraulic testing machine was used for the uniaxial compression strength (UCS) tests, fitted with a 50-kN capacity and 0.006-kN resolution load cell (Figure 1a). For reproducibility reasons, each UCS result is the average of three tested specimens. The tests were carried out under monotonic displacement control, at a rate of 0.1 mm/min. This speed is slower than the value recommended by ASTM 1633 (1996), so that it could be possible to perform small unload-reload cycles. Local deformation transducers (LDTs) were used with the UCS tests for increased strain measurement accuracy (Goto et al., 1991; Hayano et al., 1997) and, consequently, more reliable unload-reload stiffness moduli (Figure1b). These small unload-reload cycles were included in some UCS tests, at 15%, 30% and 60% of the expected uniaxial compression strength. The cycle amplitude (q_{cyc}^{max}-q_{cyc}^{min}) was established at 20% of the maximum deviator stress of each cycle (q_{cyc}^{max}).

Triaxial tests were performed using Hall-effect Transducers (Clayton et al., 1989) glued directly onto the specimen membrane (Figure 2). The specimens were saturated applying a back-pressure of 500 kPa, anisotropically consolidated considering a coefficient of earth pressure at rest (K_0) of 0.5, and sheared under displacement control at a rate of 0.01 mm/min. During the triaxial tests, unload-reload cycles were performed at 5%, 15%, 30% and 60% of the corresponding unconfined compressive strength, assuming that this value is a lower bound estimate of the peak deviator stress. A large amplitude (q_{cyc}^{max}-q_{cyc}^{min}) of 90% of the q_{cyc}^{max} was used, allowing a clear definition of the cycle.

Ultrasonic compression (P) and shear (S) wave velocities were measured by ultrasonic non-destructive transducers (Figure 3) in all the UCS test specimens, at the curing periods of 3, 7, 14, 21 and 28 days, and at 90 days for the long-term curing specimens. For wave generation

and acquisition, commercially available equipment was used (Figure 3a), comprising a pair of piezoelectric ultrasonic compression transducers, for measuring P-wave velocities, with a nominal frequency of 82 kHz and 30 mm in diameter; a pair of piezoelectric ultrasonic shear transducers, for measuring S-wave velocities, with a nominal frequency of 100 kHz and 35 mm in diameter; and a pulse waveform generator and data acquisition unit, equipped with an amplifier, directly logged to a PC, using specific software to operate as an oscilloscope.

The input signal was configured for an excitation voltage of 500 V and a pulse signal frequency of 82 kHz, both for P and S-wave transducers. The same frequency was used for both transducers since this is the closest frequency available in the function generator. Calibration of each pair of transducers was achieved by measuring the wave velocity through a calibration rod, with known density and wave velocity. The measurements were taken along the longitudinal axis of the specimens, with the specimen vertically aligned and the transducers installed on opposite faces. Therefore, the path length corresponded to the height of the specimens of approximately 140 mm. The exact travel length and the weight of each specimen were measured before each reading, with a precision of ±1%. In terms of wave propagation, the transmitter was located at the bottom of the specimen, while the receiver was at the top end. The acoustic coupling between the transducers and the specimen during the measurement was ensured by a layer of ultrasound conductive gel. Furthermore, the transducers were firmly and uniformly pressed against the top surface of the specimen, by the use of a 1 kg disk (Figure 3b) assuring a similar pressure on the transducers throughout the entire experimental program. The readings were taken at generic curing periods of 3, 7, 14, 21, 28 and 90 days. Each presented result corresponds to the average of at least ten consecutive pulse velocity readings.

Results

Assessment of stiffness by compression tests

The unload-reloading cycles performed on the unconfined compression tests allowed the evaluation of the unload-reload modulus (E_{ur}) at three different strain levels, as expressed in Figure 4 for mixture M2 after 90 days curing. From the stress-strain curves the secant stiffness modulus was determined, using the values plotted in Figure 5 against the deviator stress q normalized by its peak value (q_{peak}). The secant moduli are significantly higher in the alkali activated mixtures than in non-activated soil-ash specimens. A clear difference was also observed between the two curing times (28 and 90 days) at all stages of these UCS tests, including at peak (where bonding has been partially destroyed) meaning that a strong type of bonding is present (Cuccovillo and Coop, 1999). On the other hand, the stiffness degradation pattern appears to be steeper at 90 days than at 28 days, as typically happens when cementation increases (Leroueil and Vaughan, 1990, Viana da Fonseca et al., 2011).

Triaxial test results showed very stiff stress-strain curves, as illustrated in Figure 6. Although large cycles were performed, resulting in considerable yielding, an attempt was made to recover the elastic modulus considering the initial part of the unloading branch, as reported in Gomes Correia et al. (2004). Figure 7 illustrates this analysis for one of the tests, namely the test of M2 specimen at σ_{V0} = 50 kPa and σ_{H0} = 25 kPa.

As presented for the UCS, the secant modulus evolution during the triaxial compression tests was also plotted against q/q_{peak} (Figure 8). The data is very clear indicating that M1 mixture is definitely the stiffer, and that the confining stress contributed to an increase in stiffness. This shows that strong cemented bonds (as it is the case in M1) do not break when the confining stress is applied. In the other mixtures the results are not so evident and it is possible that a

weaker type of cementation is present resulting in some damage of cemented bonds due to confining stress, especially at M3. However, more results were needed to confirm this.

Assessment of stiffness by compression and shear wave measurements

Compression and shear wave velocities (P and S waves, respectively) were used to evaluate the development and evolution of the elastic stiffness of the cemented specimens to be tested in unconfined compression, throughout curing time. This was possible by the non-destructive nature of these ultrasonic wave measurements. Figure 9 shows the obtained output signal for P and S waves, indicating the propagation time registered in each measurement, using a classical time-domain approach. The determination of P-wave travel time is straightforward, corresponding to the first break of the received wave signal, as clearly indicated in Figure 9a). On the other hand, the selection of the shear wave arrival is slightly more complex, due to the interference of compressional waves and near-field effects in the received signal, as previously recognized by other authors (Arroyo et al., 2003; Viana da Fonseca et al., 2009). As a result, S-wave arrival was defined as the first major downward break (the polarity of the signals was determined during calibration), corresponding to the beginning of a low frequency wave, typical of shear waves, as evident in Figure 9b.

From the theory of elasticity, is it well known that compression and shear wave velocities are related to the confined (M_0) and shear (G_0) moduli, respectively, according to Equations (1) and (2).

$$\boldsymbol{M_0 = \rho V_P^2} \quad (1)$$

$$\boldsymbol{G_0 = \rho V_S^2} \quad (2)$$

where ρ is the bulk density of the material. Equation (3) provides the Poisson's ratio value (ν), from which the dynamic Young's modulus (E_0) can be derived, using Equation (4).

$$\nu = \frac{\left(\frac{V_P}{V_S}\right)^2 - 2}{2\left(\frac{V_P}{V_S}\right)^2 - 2} \quad (3)$$

$$E_0 = 2G_0\,(1 + \nu) \quad (4)$$

Figure 10 and 11 illustrate the evolution of these elastic parameters with curing time for the three different mixtures up to 90 days. Three specimens were molded for each mixture as expressed by the symbols and the average line is plotted for a clear comparison. A significant evolution of these moduli with curing time has been found. M1 and M3 mixtures have a parallel linear trend, although M1 presents higher stiffness evolution. M2 mixture consistently shows a different behavior, with a trend close to M1 at earlier curing periods but with lower stiffness values at 90 days of curing time. This may indicate that M2 mixture tends to cure at a faster rate, stabilizing at an earlier age than the other two mixtures; however, further investigation is needed to confirm this statement.

Poisson's ratio also shows an interesting trend slightly reducing at shorter curing times and then increasing up to 0.25 for M1 and M2 mixtures and 0.3 for M3. Since this has been consistently observed in all specimens, the inflexion point may be associated with the onset of the chemical reactions that create the geopolymeric gel bonding the soil particles. The curing process is associated to the formation of new bonds between particles, creating new blocks of particles which become larger with time. The increase of the dynamic Poisson ratio value after 7 days may be associated to the deformation of those blocks when loaded. In order to understand when this increase of Poisson ratio value will stop, a M1 specimen was molded specifically for this

purpose and left to cure for a year. P and S waves were measured in this specimen at 7, 75, 90, 120, 180, 300 and 365 days. The Poisson ratio curve obtained from those measurements is plotted in Figure 12 being clear that after 90 days (the higher curing time of the previous figure) the Poisson ratio tends to decrease and stabilize around 0.22. With the development of the curing process, the cementation tends to homogenize the structure creating a matrix close to what is found in concrete, dropping the Poisson's ratio values to around 0.20, close to the value of integer cemented aggregates.

Discussion

This section primarily presents the comparison and correlation between stiffness properties obtained from dynamic, cyclic and static mechanical tests at different strain levels. Table 2 summarizes the data obtained in those tests for the three mixtures at 28 and 90 days of curing, that is the dynamic Young's modulus (E_0), the unload-reload modulus obtained in the cycles (E_{ur}) and the initial tangent stiffness obtained by the initial linear trend of the stress-strain curve (E_{t0}). From the data at 28 days, it is clear that M1 shows higher stiffness than M2 which is also stiffer than M3. At 90 days, the seismic wave measurements show higher stiffness in M3 than in M2.

Due to the very low strain level involved in seismic wave measurements, E_0 corresponds to the higher stiffness modulus under purely elastic conditions. However, some unload-reload modulus, performed during triaxial tests at certain stress state in well controlled conditions, have reached very high values similar to E_0. In fact, the triaxial test data has to be analyzed taking into account the effect of the confinement stress state to compare with both the dynamic and UCS tests which were performed with no confinement. Instead of normalizing the secant

stiffness modulus (E_{sec}) by the corresponding effective stress, the E_{sec} was divided by an elastic stiffness modulus as suggested by Vardanega and Bolton (2013). Since E_0 is, in average, almost twice the initial tangent moduli of the UCS test (Table 2), and thus considerably different from the secant stiffness modulus, the E_{t0} was selected for the normalization of both UCS and triaxial test data.

The secant modulus from triaxial tests was therefore divided by the corresponding E_{t0} presented in Table 2 so that the degradation pattern of each triaxial test could be analyzed and compared with the others (Figure 13). For the low stress level, M1 mixture shows higher normalized stiffness modulus than the other mixtures. However, that does not happen for the other stress states. In fact it is interesting to notice that mixtures with lower stiffness modulus (such as M3) have less steeper degradation curves, meaning that a reduction in stiffness may be associated to a more ductile behavior conversely to the stiffer and fragile mixtures. This is very important because in some applications, such as road platforms, it may be better to have ductile behavior to avoid cracking by fatigue. In any case, considering the slow curing rate of these material, this needs to be confirmed for higher curing times.

Additionally, the UCS test results previously presented in Figure 5 for the cemented soil mixtures were normalized by the corresponding E_{t0} values in order to more clearly observe the degradation pattern of each mixture (Figure 14). The normalization of the stiffness curves enables an easier comparison between the degradation patterns of all the mixtures confirming the indications observed in Figure 5. The mixtures at 90 days, and especially M1, have clearly higher normalized modulus than the same mixtures at 28 days. This is a clear evidence of the slow rate of this cementation process and an important indication of the need to consider longer

curing periods for the correct characterization of the stiffness and strength properties of these alkali activated mixtures.

The unconfined compression tests results and the seismic wave measurements were analyzed together by calculating the ratio of the secant modulus at 10% of the peak deviator stress ($E_{sec10\%}$) from UCS with the maximum Young's modulus ($E_{sec10\%}/E_0$). This ratio presented in Table 3 gives a quantification of the degradation degree of the material, and $E_{sec10\%}$ was selected since it is a well-defined value currently used for design purposes. The ratios between these moduli reflect that M2 evidences a stiffer response at 28 days due to its faster curing rate, as already noted in the dynamic stiffness measurements, illustrated in Figures 8 and 9. It is also worth noting that the normalized ratio of the stiffer mixture (M1) is clearly lower than M2 at 28 days, inverting their relative position at 90 days, due to its stronger cementation. Comparing both curing times, is it clear that the ratio increases with longer curing periods, which is in agreement with the stiffness increase.

However, this ratio does not take into account the strain level at 10% of the peak deviator stress. Since each mixture has a different peak value, $E_{sec10\%}$ is measured at different deviator stresses and consequently at different strain levels. For that reason, the ratio $E_{sec10\%}/E_0$ was plotted against the average strain at that stress level, for each particular mixture, as represented in Figure 15. The data was separated by curing time (at 28 and 90 days in Figure 15a, for all mixtures) and by mixture (M1, M2 and M3 in Figure 15b, for both curing times). For each case, a power law ($E_{sec10\%}/E_0 = A.\varepsilon_a^n$) was adjusted, which coefficient A and exponent n are summarized in Table 4, together with the corresponding correlation coefficient (R^2). It is interesting to notice that a much higher scatter is observed for the 28 days group ($R^2 = 0.14$) than for the 90 days group ($R^2 = 0.93$), when the bonding between particles is stronger. Analyzing the R^2 for each particular mixture (Figure 15b), which are very similar, it is possible

to conclude that the significant difference between the R^2 values obtained in Figure 15a (for 28 and 90 days curing) is indeed a consequence of the specimens curing time. The strong correlation coefficients obtained (between 0.74 and 0.81), is a good indication of the adequacy of dynamic measurements in the prediction of stiffness moduli at these strain ranges.

It is also worth addressing in this discussion section, the comparison of these results with conventional soil-cement data obtained with the same soil and several cement contents and void ratios but similar molding procedures to the alkali activated mixtures. First, the values of the dynamic Young's modulus (E_0) of the alkali activated mixtures, obtained from the seismic wave measurements, were compared with those obtained for soil-cement mixtures, reported by Amaral (2009), in Figure 16.

The results presented in Figure 16 show that the soil-cement stiffness evolution is well represented by the ACI prediction (ACI Committee 209, 1998) developed for strength, and so, this expression was used to extrapolate the soil-cement results up to 90 days of curing. The soil-cement Young's modulus stabilizes around 28 days of curing, while the alkali activated mixtures show a continuous increase well beyond that mark. This is explained by the faster dissolution rate of the calcium-type glassy material, forming C-H-S gel which can be found in cement hydration, which is a distinct cementation process of these alkali activated mixtures.

Conclusions

The paper highlights stiffness characteristics of a new type of cemented soil resulting from the alkaline activation of fly ash which creates a geopolymeric gel that links the soil particles. The performance of this new material was analyzed by means of unconfined compression tests, drained triaxial compression tests and seismic wave measurements, being these last two tests applied for the first time in this material. The dynamic, cyclic and static mechanical tests show a significant increase in stiffness with curing time, even beyond the 28 days of curing period. M1 mixture showed a very strong type of cementation which does not seem to be significantly affected by the confining stress nor the yielding prior to peak since very high stiffness modulus are obtained in such conditions. However, being very stiff M1 is also very fragile after the cementation bonds are broken, conversely to the other mixtures.

Compression and shear seismic wave measurements allowed the evaluation of the dynamic Poisson's ratio which revealed very interesting results. A slight decrease of this ratio in the first days of curing followed systematically by an increase of Poisson's ratio value indicated that curing may only be particularly effective after the first 7 days, conversely to what is observed in soil-cement specimens. This increase in the Poisson ratio value slightly decreases after 90 days of curing stabilizing at values close to 0.2, typical of concrete.

The unconfined test secant modulus at 10% of the peak deviator stress ($E_{sec10\%}$) normalized by the maximum Young's modulus (E_0) was well adjusted by a power law in two different situations: for all mixtures at 90 days curing, and for each individual mixture considering all curing periods. This indicates that the stiffness modulus at these strain levels can be well predicted by the dynamic measurements for each mixture. Moreover, since the cemented

behavior tends to become more uniform with curing time, the long term stiffness modulus can be also well predicted by dynamic measurements, independently of the type of mixture.

The results point towards a similar type of cementation in both soil-cement and alkali activated mixtures, characterized by a significant increase in stiffness. The most important difference in both types of bonding lies on the curing process, since cement presents a significant increase at early ages stabilizing at 28 days, while alkali activated soil-ash mixtures show a more gradual and continuous increase, almost doubling its stiffness from 28 days to 90 days of curing.

Acknowledgements

The authors would like to acknowledge the company Pegop – Energia Eléctrica SA which runs the thermoelectric power plant of Pego, for the supply of fly ash;; and to ANI (Agência de Inovação) for their support through ECOSOLO project (ref. 38899/2012). A particular acknowledgment is also due to the Portuguese Science and Technology Foundation for their financial support through the SFRH/BPD/85863/2012 scholarship funded by the Portuguese Ministry of Science and Technology (MCTES) and the European Social Fund (FSE) by POCH program.

References

ACI Committee 209 (1998). Prediction of Creep, Shrinkage, and Temperature Effects in Concrete Structures. Committee Report ACI 209R-92. ACI Man. Concr. Pract. Part I

Amaral, M.F. (2009). Dynamic shear modulus evaluation in soil–cement mixtures using time domain ultrasonic impulses and recording the resonant frequencies with Fourier spectral analysis - MSc Thesis (in Portuguese). Faculty of Engineering of University of Porto.

Arroyo, M., Wood, D.M., Greening, P.D. (2003). Source near-field effects and pulse tests in soil samples. Géotechnique 53 (3), 337-345

ASTM (1996). D 1633-96. Standard test method for compressive strength of molded soil-cement cylinders. Annual Book of Standards, vol. 04.08

ASTM (2003). C618. Standard Specification for Coal Fly Ash and Raw or Calcined Natural Pozzolan for Use in Concrete. Annual Book of Standards, vol. 04.02

ASTM (2011) D 7181. Method for Consolidated Drained Triaxial Compression Test for Soils. Annual Book of Standards, vol. 04.09

Bernal, S., R. M. Gutiérrez, A. L. Pedraza and J. L. Provis (2011). Effect of binder content on the performance of alkali-activated slag concretes. Cement and concrete research 41, 1-8.

Camusso, M. and M. Barla (2009). Microparameters Calibration for Loose and Cemented Soil When Using Particle Methods. International Journal of Geomechanics 9(5), 217-229.

Chen, R., Lee, I., Zhang, L. (2014). Biopolymer Stabilization of Mine Tailings for Dust Control. J. Geotech. Geoenvironmental Eng. (doi:10.1061/(ASCE)GT.1943-5606.0001240)

Cheng, L., Cord-Ruwisch, R., Shahin, M.A. (2013). Cementation of sand soil by microbially induced calcite precipitation at various degrees of saturation. Can. Geotech. J. 50, 81–90.

413 Clayton, C., Khatrush, S., Bica, A., Siddique, A. (1989). The Use of Hall-effect Semiconductors
414 in Geotechnical Instrumentation. Geotech. Test. J. 12, 69–76.

415 Consoli, N., Viana da Fonseca, A., Cruz, R., Rios, S. (2011). Voids/Cement ratio controlling
416 tensile strength of cement treated soils. Journal of Geotechnical and Environmental
417 Engineering 137(11), 1126-1131 (doi:10.1061/(ASCE)GT.1943-5606.0000524)

418 Cristelo, N., S. Glendinning and A. Teixeira Pinto (2011). Deep soft soil improvement by
419 alkaline activation. Ground Improvement 164(GI2), 73-82.

420 Cristelo, N., S. Glendinning, L. Fernandes and A. Teixeira Pinto (2013). Effects of alkaline-
421 activated fly ash and Portland cement on soft soil stabilisation. Acta Geotechnica 8, 395-
422 405.

423 Cuccovillo, T., Coop, M.R. (1999). On the mechanics of structured sands. Géotechnique 49,
424 741–760.

425 Dupas, J.-M., Pecker, A. (1979). Static and Dynamic Properties of Sand-Cement. J. Geotech.
426 Eng. Div. 105, 419–436.

427 Gomes Correia, A., Viana da Fonseca, A., Gambin, M. (2004). Routine and advanced analysis
428 of mechanical in situ tests. Results on saprolitic soils from granites more or less mixed in
429 Portugal, in: Proc. ISC-2 on Geotechnical and Geophysical Site Characterization, 75–95.

430 Goto, S., Tatsuoka, F., Shibuya, S., Kim, Y., Sato, T. (1991). A Simple Gauge for Local Small
431 Strain Measurements in the Laboratory. Soils Found. 31, 169–180.

432 Hayano, K., Tatsuoka, F., Sato, T. (1997). Deformation characteristics of a sedimentary soft
433 mudstone from triaxial compression tests using rectangular prism specimens.
434 Géotechnique 47, 439–449.

435 Hossain, M. and Yin, J. (2015). Dilatancy and Strength of an Unsaturated Soil-Cement Interface
436 in Direct Shear Tests. International Journal of Geomechanics, 15(5)

437 10.1061/(ASCE)GM.1943-5622.0000428 , 04014081.

438 Kang, X., L. Ge and W. C. Liao (2016). Cement Hydration–Based Micromechanics Modeling
439 of the Time-Dependent Small-Strain Stiffness of Fly Ash–Stabilized Soils. International
440 Journal of Geomechanics 0(0): 04015071.

441 Khatami, H.R., O'Kelly, B.C. (2013). Improving Mechanical Properties of Sand Using
442 Biopolymers. J. Geotech. Geoenvironmental Eng. 139, 1402–1406.

443 Leroueil, S., Vaughan, P.R. (1990). The general and congruent effects of structure in natural
444 soils and weak rocks. Géotechnique 40, 467–488.

445 Little, D. (1995). Handbook for stabilization of pavement subgrades and base courses with lime.
446 Kendall/Hunt Pub. Co., Dubuque Iowa.

447 Palomo, A., M. W. Grutzeck and M. T. Blanco (1999). Alkali-activated fly ashes. A cement for
448 the future. Cement and concrete research 29: 1323-1329.Rios, S., Viana da Fonseca, A.
449 and Baudet, B. (2012). The effect of the porosity/cement ratio on the compression
450 behaviour of cemented soil. Journal of Geotechnical and Environmental Engineering,
451 138(11), 1422–1426, doi: 10.1061/(ASCE)GT.1943-5606.0000698

452 Rahimi, M., D. Chan and A. Nouri (2016). Bounding Surface Constitutive Model for Cemented
453 Sand under Monotonic Loading. International Journal of Geomechanics 16(2): 04015049.

454 Rios, S., Viana da Fonseca, A. and Baudet, B. (2012). The effect of the porosity/cement ratio
455 on the compression behaviour of cemented soil. Journal of Geotechnical and
456 Environmental Engineering, 138(11), 1422–1426, doi: 10.1061/(ASCE)GT.1943-
457 5606.0000698

458 Rios, S., Viana da Fonseca, A. and Baudet, B. (2014). On the shearing behaviour of an
459 artificially cemented soil. Acta Geotechnica, 9(2), 215-226, doi: 10.1007/s11440-013-
460 0242-7

461 Rios, S., Cristelo, C., Viana da Fonseca, A., Ferreira, C. (2016). Structural Performance of
462 Alkali Activated Soil-Ash versus Soil-Cement. Journal of Materials in Civil Engineering,
463 28(2), DOI: 10.1061/(ASCE)MT.1943-5533.0001398

464 Sauceda, M., Johnson, D.W., Huang, J., Bin-Shafique, S., Sponsel, V.M., Appleford, M.,
465 (2014). Soil-Strength Enhancements from Polymer-Infused Roots. J. Geotech.
466 Geoenvironmental Eng. 140(2), (doi:10.1061/(ASCE)GT.1943-5606.0000999)

467 Scrivener, K. L., & Kirkpatrick, R. J. (2008). Innovation in use and research on cementitious
468 material. Cement and concrete research, 38, 128-136.

469 Sukmak, P., S. Horpibulsuk and S.-L. Shen (2013). Strength development in clay–fly ash
470 geopolymer. Construction and Building Materials 40(0), 566-574.

471 Turner, L.K., Collins, F.G. (2013). Carbon dioxide equivalent (CO2-e) emissions: A
472 comparison between geopolymer and OPC cement concrete. Construction and Building
473 Materials 43, 125–130.

474 Vardanega, P. J. and M. D. Bolton (2013). Stiffness of Clays and Silts: Normalizing Shear
475 Modulus and Shear Strain. Journal of Geotechnical and Geoenvironmental Engineering
476 139(9), 1575-1589.

477 Viana da Fonseca, A., Ferreira, C. and Fahey, M. (2009). A Framework Interpreting Bender
478 Element Tests, Combining Time-Domain and Frequency-Domain Methods. Geotechnical
479 testing Journal, 32 (2), 1-17

480 Viana da Fonseca, A., Coop, M.R., Fahey, M., and Consoli, N.C. (2011). The interpretation of
481 conventional and non-conventional laboratory tests for challenging geotechnical
482 problems, in: Proc. of International Symposium on Deformation Characteristics of
483 Geomaterials, Seoul, 1-36.

484 Viana da Fonseca, A., Rios, S., Amaral, M. F. (2013). Structural anisotropy by static

compaction, Engineering Geology, 154, 89-97, http://dx.doi.org/10.1016/j.enggeo.2012.11.012

Yi, Y., Liska, M., Unluer, C., Al-Tabbaa, A. (2013). Carbonating magnesia for soil stabilization. Can. Geotech. J. 50, 899–905.

Tables

Table 1: Characterization of all the mixtures analyzed

ID	Ash / solids (wt.)	Na_2O / ash (wt.)	NaOH concent. (molal)	Water content (%)	Activ. content (%) [a]	Activ. / ash (wt.)	Dry unit weight (kN/m^3) [b]	SiO_2 / Na_2O (wt.) [c]
M01	0.15	-	-	11.7	-	-	18.22	-
M02	0.20	-	-	15.6	-	-	17.08	-
M03	0.25	-	-	19.5	-	-	16.04	-
M1	0.15	0.125	7.5	8.8	11.7	0.781	18.22	0.552
M2	0.20	0.125	7.5	11.7	15.6	0.781	17.08	0.552
M3	0.25	0.125	7.5	14.7	19.5	0.781	16.04	0.552

[a] For a SS/SH mass ratio of 0.5; [b] For a unit weight of 20 kN/m^3; [c] Quantities from the activator

Table 2: Stiffness modulus of the analyzed mixtures from dynamic, cyclic and static tests

Type of tests	Parameter	28 days			90 days		
		M1	M2	M3	M1	M2	M3
Dynamic tests	E_0 (MPa)	3239	2831	2597	7123	5852	5924
UCS tests	E_{ur} (MPa)	-	-	-	-	[3954-5027]	[2000-3972]
	E_{t0} (MPa)	1452	1274	1010	3740	3016	2696
Triaxial Tests	E_{ur} (MPa)	[2220-3165]	[1118-2030]	[500-2560]	-		
	E_{t0} (MPa)	[1950-4050]	[982-1347]	[587-1865]			

Table 3: Stiffness modulus of the analyzed mixtures

Parameter	28 days			90 days		
	M1	M2	M3	M1	M2	M3
E_0 (MPa)	3239.48	2831.27	2596.89	7123.15	5852.23	5924.41
$E_{sec10\%}$ (MPa)	1378.58	1344.85	876.46	3629.85	2825.00	2556.17
$E_{sec10\%}/E_0$	0.43	0.47	0.34	0.51	0.48	0.43

Table 4: Power fit constants

Source data (Fig. 12)	Constant A	Exponent n	R^2
28 d	0.0117	-0.40	0.14
90 d	0.0002	-0.88	0.93
M1	0.001	-0.69	0.74
M2	0.0003	-0.82	0.81
M3	0.003	-0.80	0.74

Figures

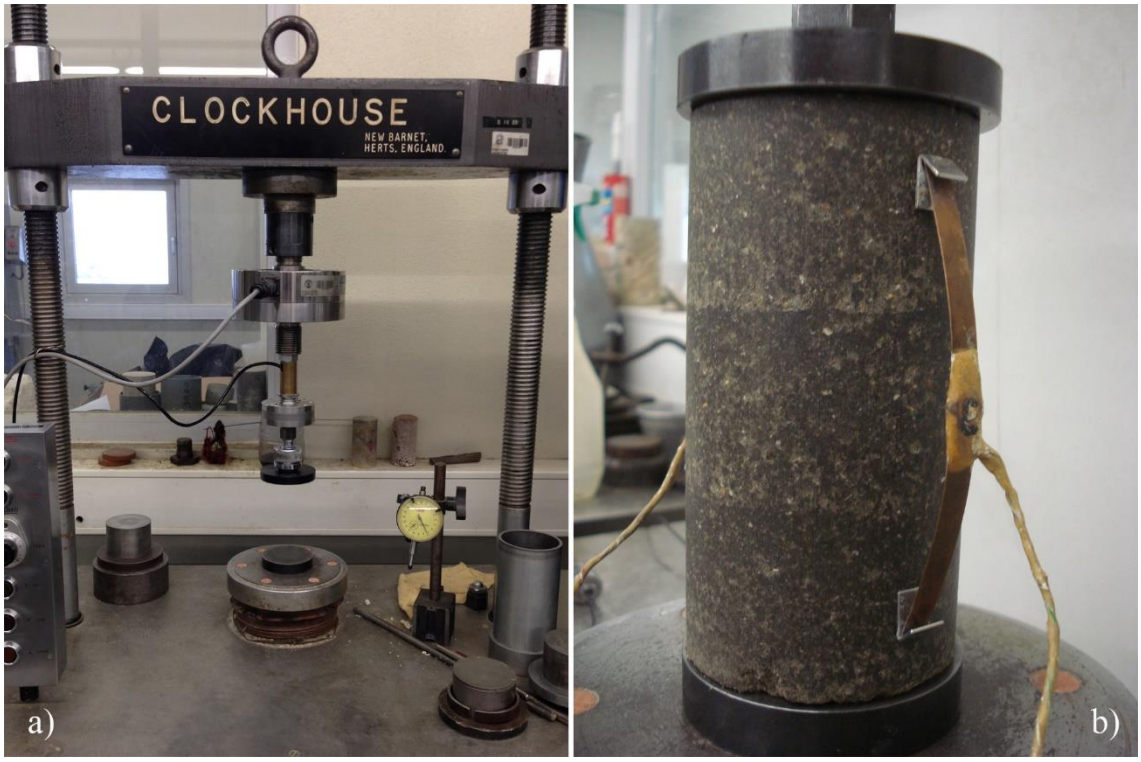

Figure 1: (a) Load frame for uniaxial compression tests; (b) strain measurement setup

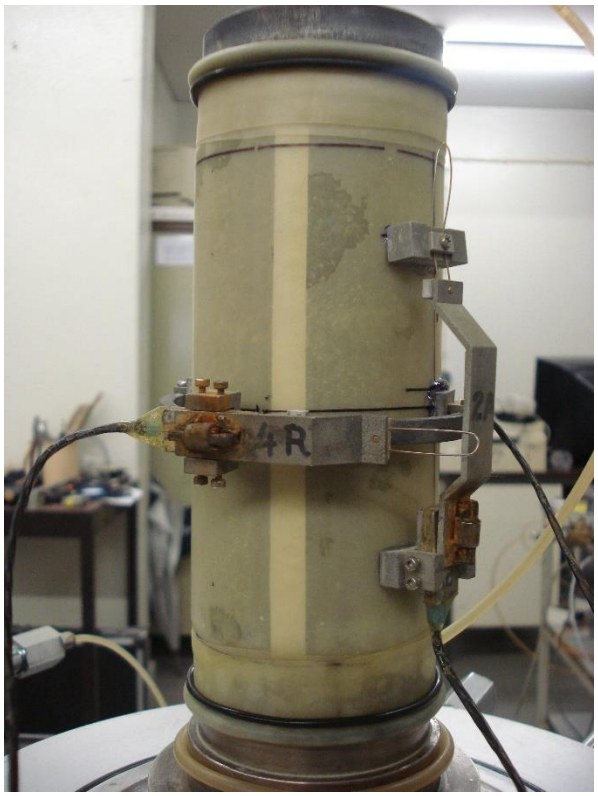

Figure 2: Triaxial compression strain measurement setup

Figure 3: Seismic P- and S-wave velocity measurement equipment (a) and setup (b)

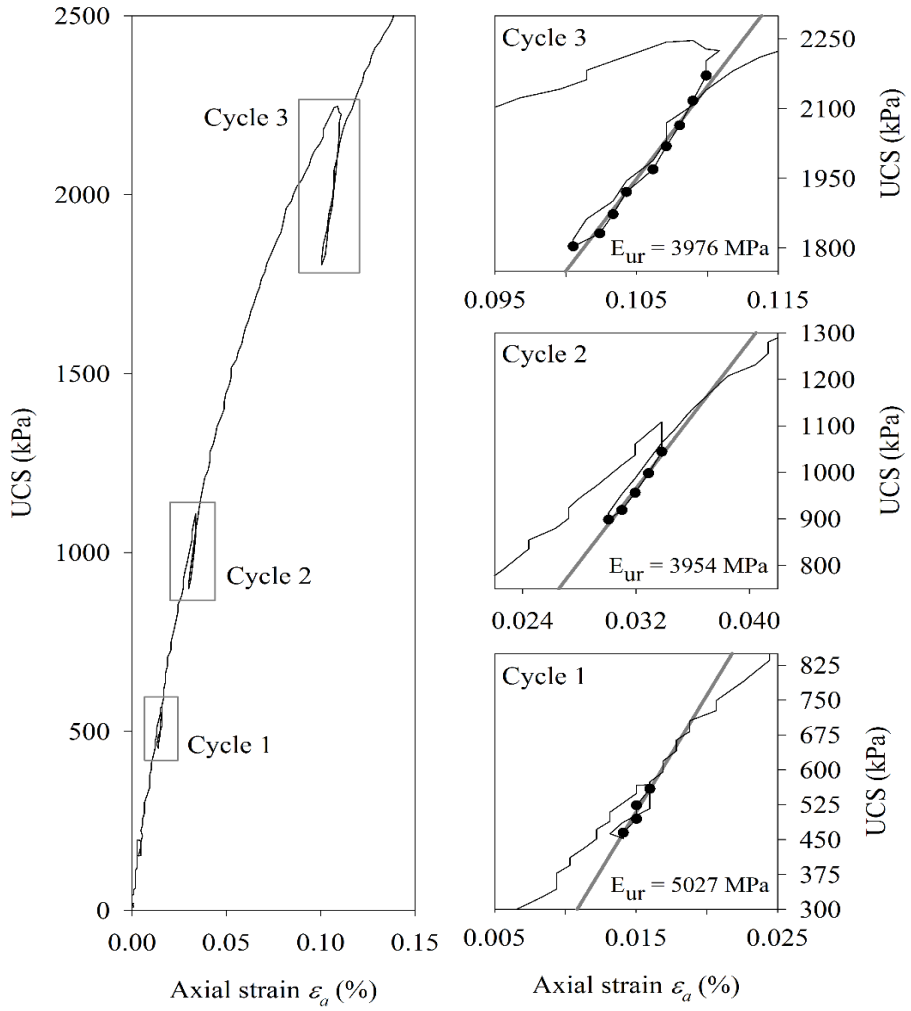

Figure 4: Stiffness modulus obtained from cycles performed during the unconfined compressive strength test of one of the M2 specimens after 90 days curing

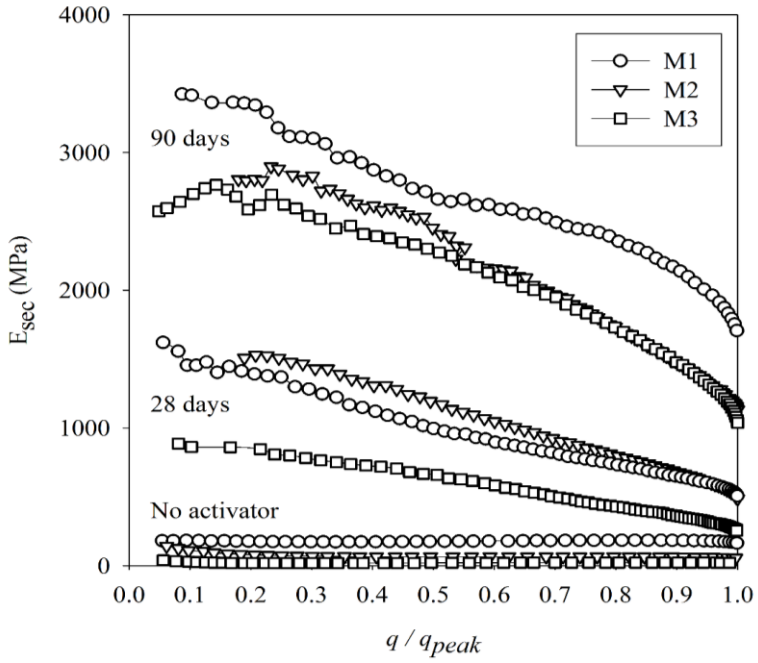

517

518 Figure 5: Evolution of the secant stiffness modulus throughout the unconfined compression test

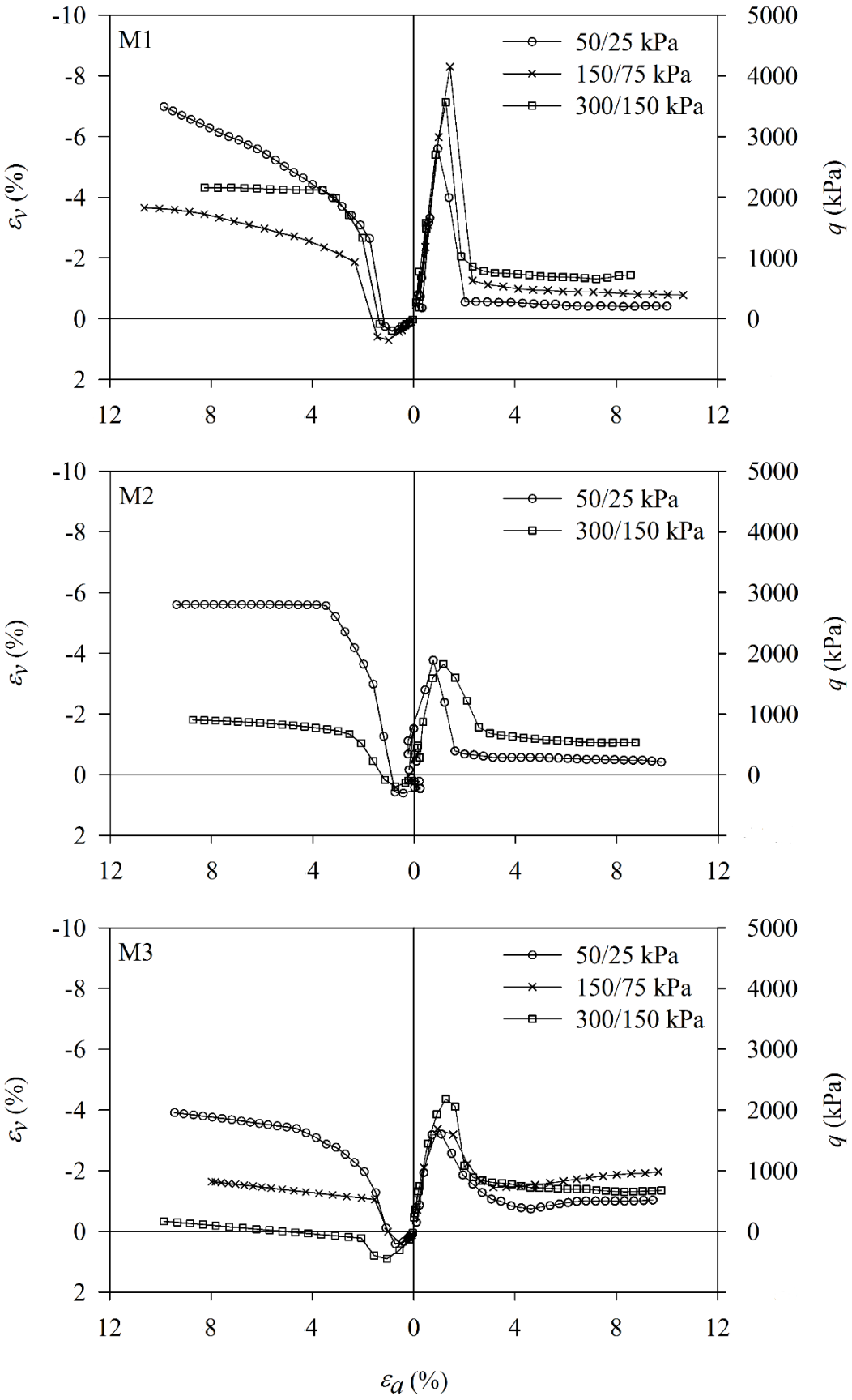

519

520 Figure 6: Stress-strain-volume curves obtained in drained triaxial compression tests of stabilized soil for the
521 three mixtures (M1 M2 and M3).

522

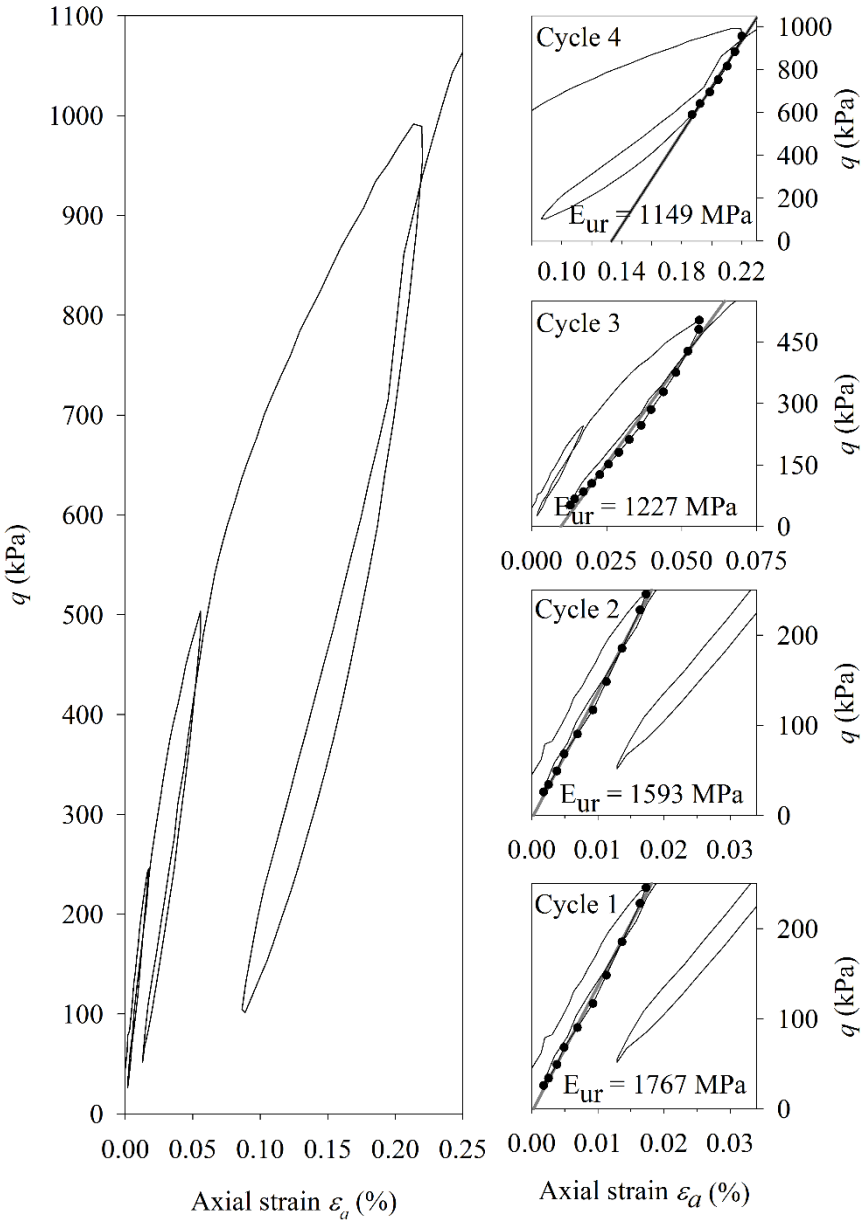

Figure 7: Stiffness modulus obtained from the cycles performed during the triaxial compression test of M2 specimen at σ_{V0} = 50 kPa and σ_{H0} = 25 kPa

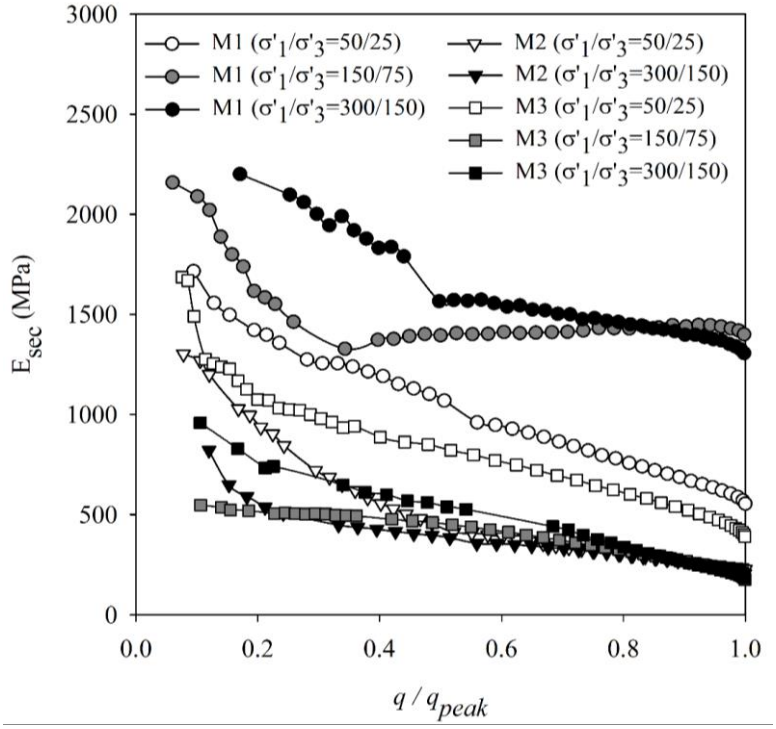

Figure 8: Evolution of the secant stiffness modulus for the different triaxial compression tests

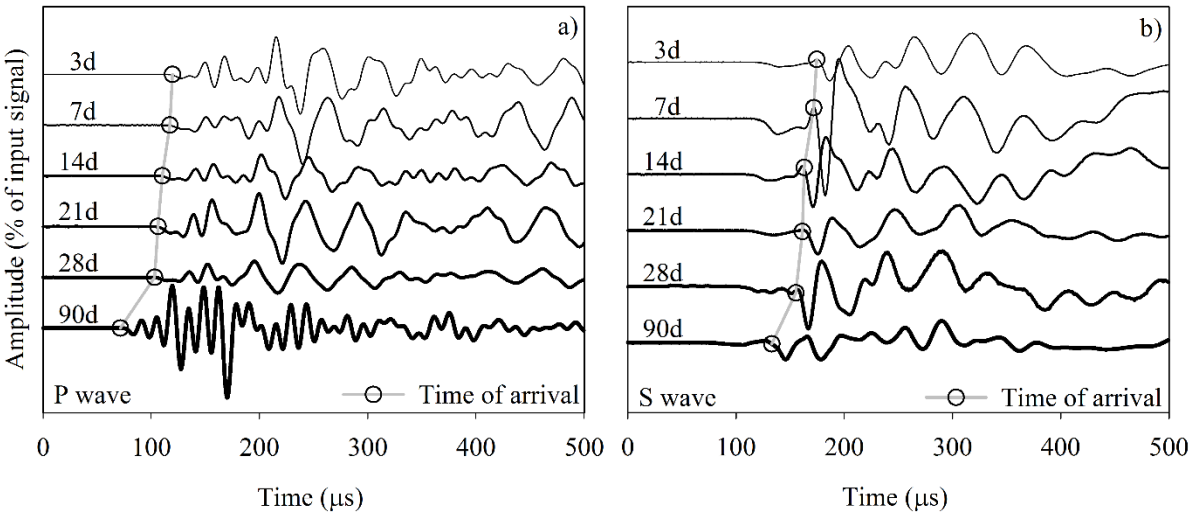

Figure 9: Seismic wave measurements: a) determination of P-wave propagation time; b) determination of S-wave propagation time

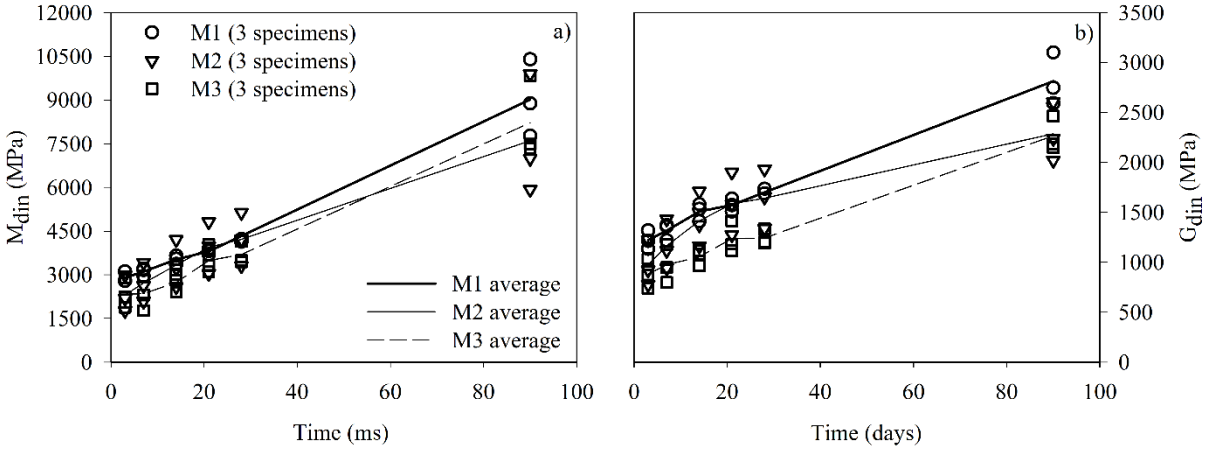

Figure 10: Stiffness evolution with time: a) confined modulus, b) shear modulus

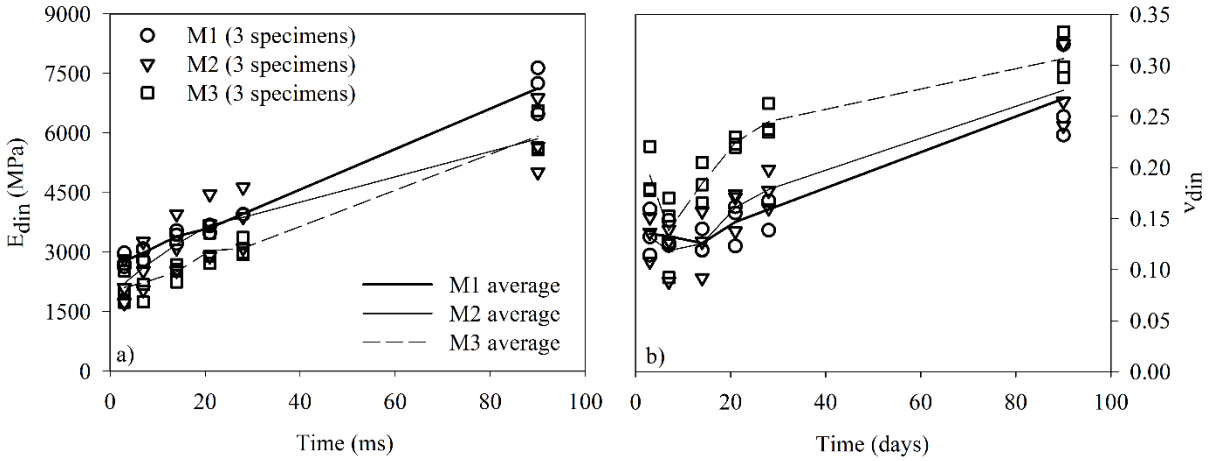

Figure 11: Dynamic Young's modulus (a) and Poisson's ratio (b) evolution with curing time

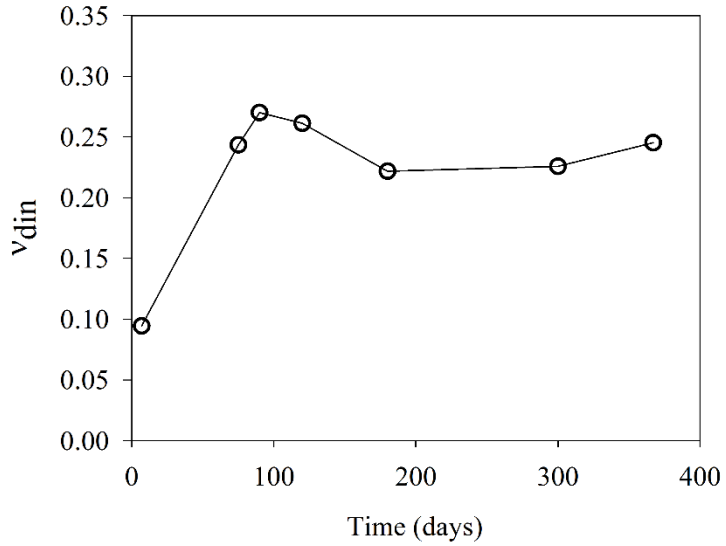

551

552 Figure 12: Poisson's ratio evolution up to 1 year of curing time

553

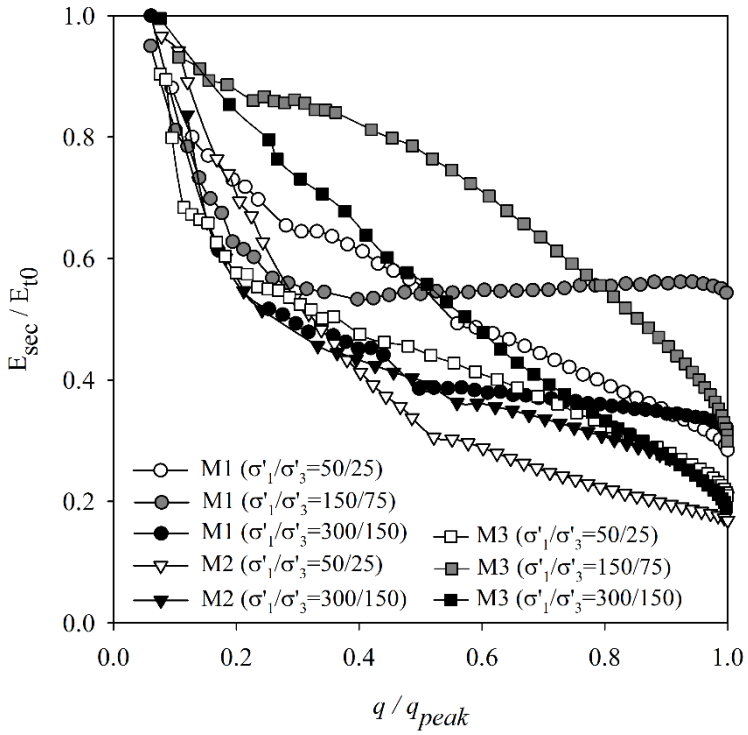

554

555 Figure 13: Evolution of the secant stiffness modulus throughout the triaxial compression tests of the three

556 mixtures

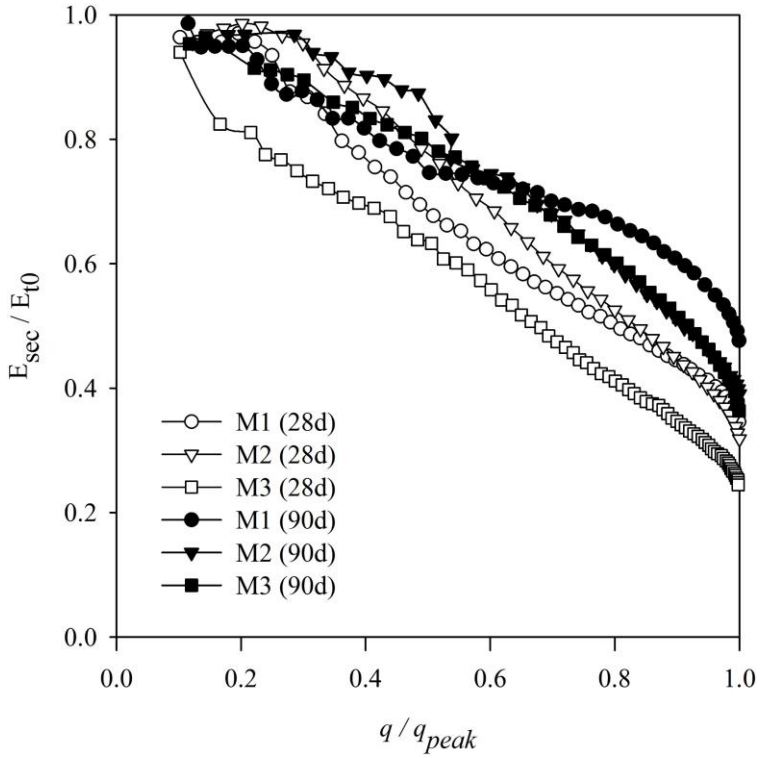

Figure 14: Evolution of the secant stiffness modulus normalized by the maximum Young's modulus throughout the unconfined compression test

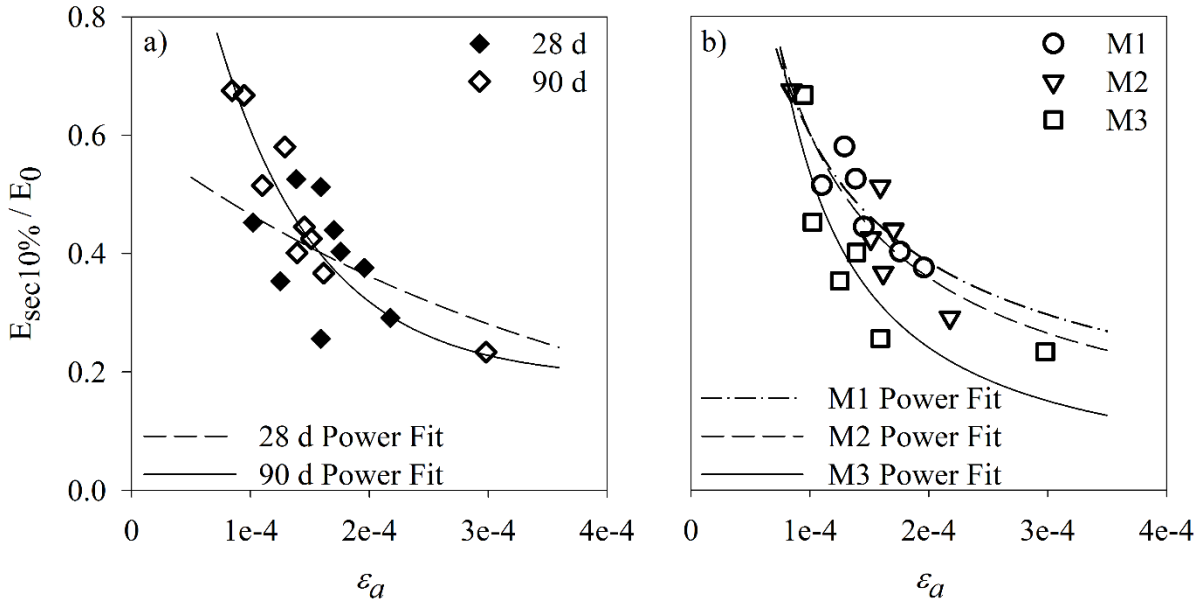

Figure 15: Normalized secant modulus at 10% of peak deviator stress against strain: a) at 28 and 90 days for all mixtures; b) for each mixture (M1, M2 and M3) for both curing times

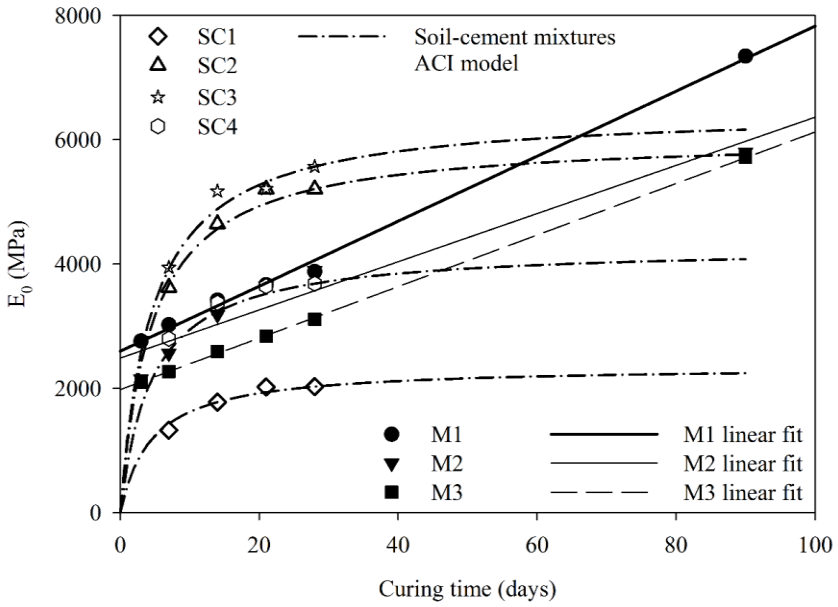

565

566 Figure 16: Dynamic Young's modulus evolution with time for soil-cement and alkali activated mixtures

567

568